Chapter 3: Particle-in-Cell Simulation of Gyro-twystron Amplifier*

*Part of this work has been published as:

A. S. Singh, S. Yuvaraj and M. Thottappan, "Analytical and PIC Simulation Studies of a Megawatt Class Gyrotwystron Amplifier," *IEEE Transactions on Electron Devices*, vol. 63, no. 10, pp. 4104-4112, Oct. 2016.

3.1 Introduction

Nowadays, the design and development of VEDs are partly or fully dependent on simulation tools. In the present chapter, 3D electromagnetic simulation of gyro-twystron has been done to validate the analytical results, which were discussed in chapter 2. The analytical development of chapter 2 leads towards the modelling and simulation of gyro-twystron amplifier. The nonlinear theory available in the literature for the study of beam wave interaction in gyro-twystron that is limited to single-mode operation, which is extended to the multimode formalism. The CST Studio Suite is chosen for 3D electromagnetic simulation as it has multimode computational capabilities.

The present chapter emphasizes the modelling and simulation of gyro-twystron amplifier to study its 3D beam-wave interaction behavoiur. In the first phase, each component of gyro-twystron is modelled independently using design parameters. Beam absent analysis, *i.e.* cold analysis of each section of gyro-twystron has been done to ensure its frequencies (operating, resonating, and cut off) and modes with quality factor. CST microwave studio is employed to study the cold propagation characteristics of the sub-assemblies of gyro-twystron. In the second phase, the electron beam is incorporated, *i.e.* hot analysis, in which the interaction of the hot electron beam and RF wave is studied using PIC simulation. To optimise the performance of gyro-twystron amplifier, various parameters are varied to maximise the performance metrics. For numerical benchmarking, an X-band gyro-twystron amplifier operating in the fundamental harmonic TE_{01} mode has been chosen. The details of electromagnetic simulation techniques and simulation study of gyro-twystron are discussed below.

3.2 Electromagnetic simulation

Manufacturing difficulties and application-specific design increases the cost of the development of VEDs. Before putting the considerable investments to experimental development and testing, virtual testing of VEDs has been done to predict the design and operating parameters. The acceptable predicted parameters of theoretical study allow for device manufacture and development [28], [92]. Electromagnetic simulation is a way of reducing the time and costs of device development [93]. In addition to preliminary calculations/predictions, the different parameters for a wide range of operations are investigated through the electromagnetic simulation tool. The 3-D simulation tool provides the virtual environment to visualize the propagation as well as the interaction of RF wave and electron beam. The 3-D simulation tool can examine the operating limits of the device and investigate the deleterious effect on device operation at above/below to predicted parameters. Above-mentioned advantages suggested that the electromagnetic simulation tools should be incorporated as an integral part of design and development study of high power gyrotron devices. Computer-aided design (CAD) tools are popular for modelling of different problems [28]. The 3-D electromagnetic model is created to achieve the background environment similar to the experimental devices, and its computational model is based on the different numerical techniques.

3.2.1 Numerical techniques

Computation of the wave equations and particle dynamics have been done using different numerical techniques. Integral and differential approaches classify numerical techniques into volume/surface integral and differential equation methods, respectively [94]. Methods of moments (MOM), multiple multi-poles (MMP) are the numerical technique employed in volume integral method. These methods employed for wave scattering problem, especially for spherical structures while null field method (NFM) as surface

integral methods employed to compute the wave scattering by a spherical problem [94]. Due to the time complexity, volume and surface integral methods are not suitable for large problems. Differential equations methods such as Finite element method (FEM), Finite-Difference Time-Domain method (FDTD) and Finite Integration Technique (FIT) discretise the solution space to calculate the wave equations. Differential equation approaches are suitable for closed space problem, and a perfectly matched layer (PML) leverages the computational complexity of the open boundary problem. In FEM, solution space is divided into subspace called element, e.g. triangle (2D), tetrahedra (3D). This frequency-domain based numerical techniques are employed in popular 3D simulation software HFSS [95]. Spatial and temporal variation of Maxwell curl equations is computed by FDTD using *Yee* cell. FDTD technique provides fast and accurate calculations for the structured Cartesian grid. With the similar discretisation method as FDTD, FIT converted Maxwell integral equations into linear equations. The interface between different media, curved boundaries and complex structures are incorporated in computation without any degradation of accuracy. Popular Electromagnetic simulation tool CST studio suite is working on finite integration technique [96]. Incorporation of particles into these field calculating numerical techniques needs particle-in-cell techniques in which the particles with similar physical charge and specific mass ratio are represented as units. This macro particle representation approach incorporated the millions of unit particles to form an electron beam, and the interaction between RF wave and the electron beam is studied using PIC technique [28]. Computation of Maxwell equations and Lorentz force equations are the core of PIC simulation. Through the current density term, fields and particle dynamics are coupled to each other in a self-consistent manner as shown in figure 3.1. Charge conservation is ensured at each node of the

solution space using the continuity equation. In solution space, the kinetic parameters of particles and field are defined in continuum space and at a discrete point, respectively.

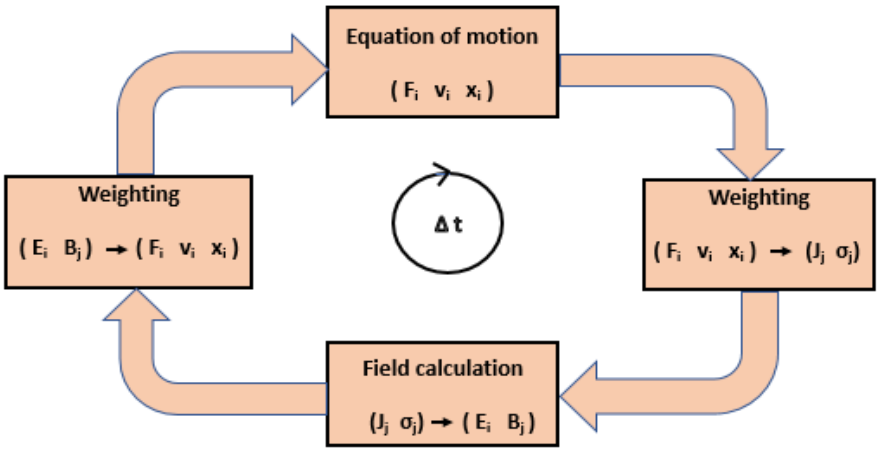

Figure 3.1 Particle in cell simulation

3.2.2 3-D simulation tool

3-D simulation studies of RF interaction structure of VEDs are divided into two phases: beam absent study and beam-wave interaction study. However, in the design and development of particle emitter and collector, the propagation of the RF wave is considered zero unlike the interaction structure analysis. For RF propagation study, CST MWS, HFSS, XFdtd and COMSOL are popular and commercially available software, which are based on FIT, FEM, FDTD and FEM with boundary element, respectively [95-98]. Among them, CST MWS provides seven solvers for a vast range of electromagnetic problem in different structures [96]. For accuracy, CST MWS employs hexahedral meshing with perfect boundary and thin sheet approximations. In Eigenmode solver, CST MWS uses either of tetrahedral meshing or hexahedral meshing. With the hexahedral meshing, CST MWS has interoperability with CST particle studio and CST Mphysics studio. With the large and versatile problem-solving approach, CST MWS is preferred over other simulation tool for the cold simulation study. Conversely, HFSS is seldom

employed to validate the RF propagation characteristics of subassemblies of the gyro-twystron amplifier.

CST PS, MAGIC 3D, VSIM and KARAT are popular commercially available simulation tools, which are used to study the beam-wave interaction mechanism using PIC technique [96],[99-101]. VSIM, KARAT and MAGIC employ PIC simulation based on different variant of FDTD techniques. VSIM tool computes the RF wave and electron beam propagation as well as the beam-wave interaction using conformal FDTD technique [100]. KARAT is fully relativistic PIC code employs FDTD with the shearing grids near to the boundary [101]. MAGIC 3D also employs FDTD PIC and integrated Maxwell's equations and Lorentz's force equation using the leapfrog time integration scheme [101]. CST particle studio is based on FIT algorithm with perfect boundary approximation [96]. PIC solver of CST particle studio is an extension of TS3 code of MAFIA tool, which was used to compute the Maxwell's equations and particle dynamics [102]. Unlike MAGIC-3D, CST PS PIC solver has multimode computational capabilities with additional advantages including particle tracking solver, wakefield solver. The particle tracking solver computes electron beam trajectories of electron gun and particle collector.

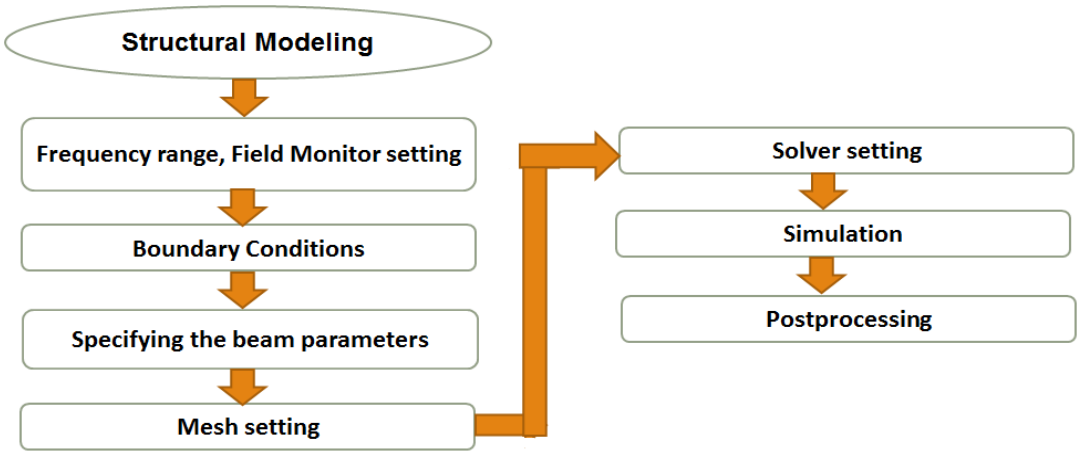

Figure 3.2 Simulation procedure for beam wave interaction study

3.3 Simulation Study of Conventional Gyro-twystron

A simulation study of conventional gyro-twystron follows the procedure as shown in Figure 3.2. Modelling of each component has been done independently, and its frequency, mode, and quality factor are ensured through the cold analysis. These individual components are added to form the hybrid gyro-twystron amplifier. Apart from the interaction structure, modelling and RF propagation characteristics study of input coupler and RF window have been discussed.

3.3.1 Modelling

To study the 3D beam-wave interaction behaviour, the RF interaction circuit has been modelled. CST studio suite provides the graphical user interface (GUI) based modelling using ACIS kernel. With the design parameters as given in chapter 2, Table 2.1, the single cavity gyro-twystron is modeled using the CST microwave studio (Figure 3.3). The modelled structure is divided with fine cells independently in x, y, and z coordinates using the inbuilt meshing technique such as hexahedral meshing in "CST Studio suite" as shown in Figure 3.4(a). The whole simulation structure is meshed with 10 cells per wavelength having a lower mesh limit of 20. This results in a smaller cell size of 0.1445mm, the largest cell size of 2.722 mm, and the total mesh cells of 2,663,424. The maximum number of meshes is decided by the constraints like the operating wavelength, simulation time, memory size, etc. Further, the boundary condition has been applied in such a way that the tangential component of the electric field vanished (E_t= 0) at the walls of the RF circuit [Figure 3.4(b)], and the background material is a vacuum. The interaction structure of gyro-twystron consists of an input cavity and an output waveguide which are separated by drift tube. Each component of gyro-twystron is modelled independently. Cavities and drift tube walls are modelled using an annealed copper, which has the conductivity (σ) of 5.8×10^7 S/m. Since, the start current is inversely related to the quality

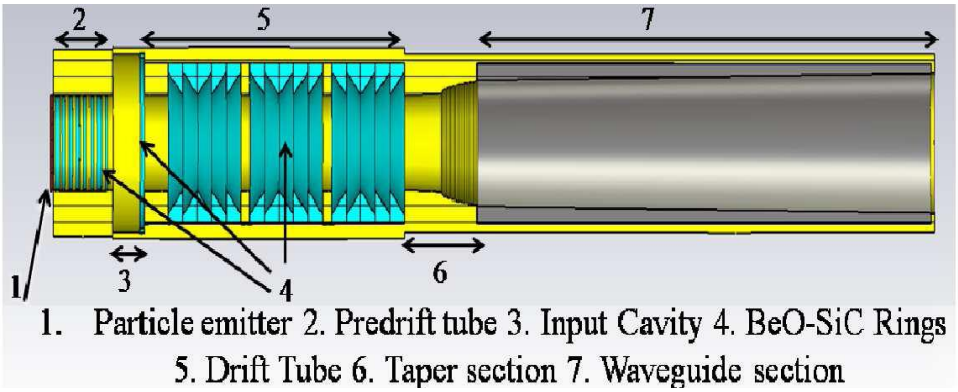

Figure 3.3 CST model of X-band unloaded gyro-twystron

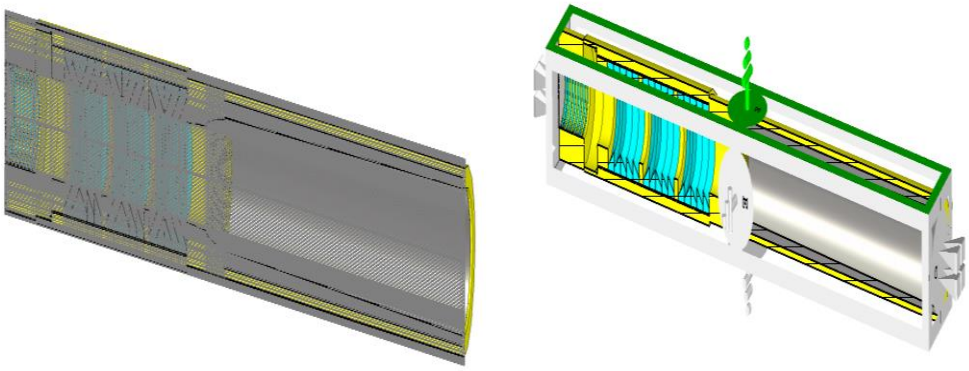

(a) (b)

Figure 3.4 (a) Mesh view, and (b) boundary condition of CST model of X-band unloaded gyro-twystron

factor (Q) of the input cavity, it is loaded with Beryllium Oxide-Silicon Carbide (BeO-SiC) dielectric rings to reduce the oscillations. The dielectric material BeO-SiC having the complex dielectric constant of 31- j13 and its loss tangent of 0.419 at 10GHz (Figure 3.5). The higher thermal conductivity of Beryllia (BeO) and its composites make them a suitable dielectric material for high power vacuum tube application. To provide the isolation between different sections of RF circuit, a field-free drift region is placed between the cavity and the waveguide. A preliminary drift located between the particle emitter and the input cavity to provide an efficient bunching at the input cavity. The pre-drift tube is realized using rings of silicon carbide impregnated beryllium oxide. In order to model the field-free drift region, the radius of the drift section is fixed such that the operating frequency is well above the cut-off frequency of the drift tube for an operating

mode. To absorb the electromagnetic (EM) fields, which are leaked into the drift section, it is loaded with the lossy ceramic rings of BeO-SiC having the length of 3 mm and the radial thickness of 1 mm. A 20 mm and 2-degree taper is followed by a 20 mm nonlinear section is present between the drift section and the output waveguide. At the end of 140 mm length of drift tube, a nonlinear taper section of 20 mm is terminated to overcome abrupt reflections. The outer radius of the waveguide is set such that the cutoff frequency of the waveguide is just below the operating frequency. To achieve the stability against competing modes, a 0.5-degree tapering is added to the output section that brings the waveguide radius to ~22mm. At the output end, a 3-degree short taper is present to introduce slight microwave reflections.

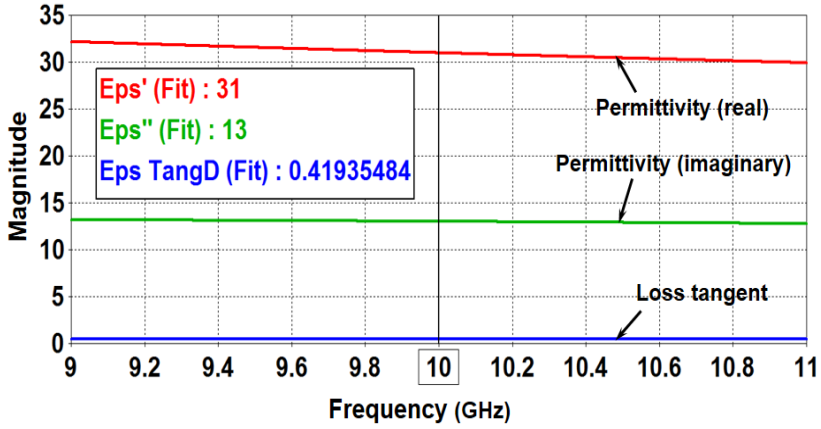

Figure 3.5 Relative dielectric properties of BeO-SiC in X-band

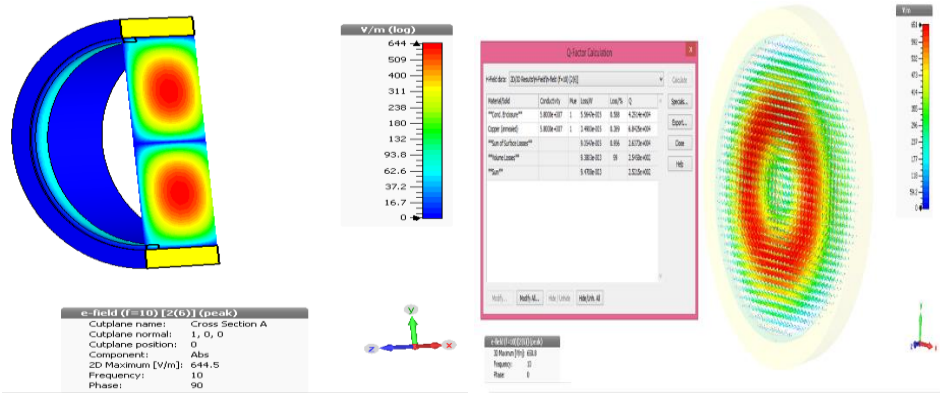

Figure 3.6 Different view of electric field confinement with quality factor

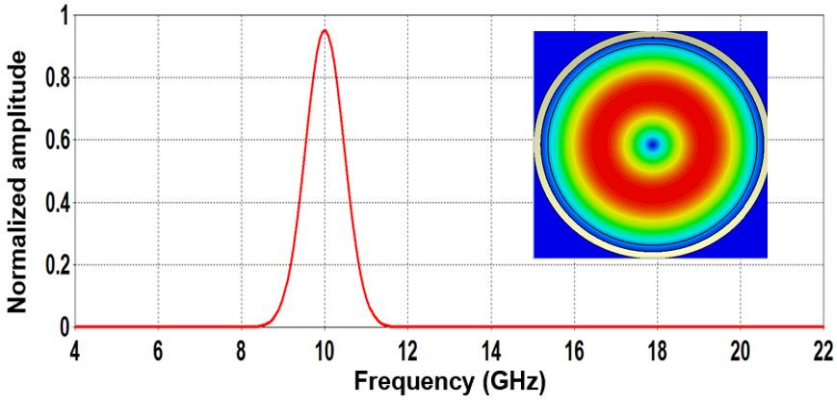

Figure 3.7 The resonating frequency of the input cavity with the contour plot

3.3.2 Beam absent study (cold simulation)

The electromagnetic characteristic of the input cavity is studied through the transient simulation without considering the electron beam (cold simulation) in "CST Microwave studio" to ensure the operating mode, frequency, and to calculate the desired *Q*-factor. Transverse electric/magnetic modes are identified by field configurations confined at resonating frequency in interaction structure. Eigenmode and transient solver are employed to identify the electric field confinement. Eigenmode solver computed the double curl of the electric field using Maxwell's curl equations, and the electric field vectors are represented at their Eigenvalue (frequency). Eigenmode solver is suitable for resonant RF structures; however, for travelling wave section, transient solver is more appropriate. Apart from the field configuration, the propagation/resonating characteristics of the interaction structure is discussed through the scattering parameters. In transient solver, two ports are created to calculate the S-parameters of devices. For metallic input cavity, the cut-off frequency of TE_{01} mode is observed at 6.6 GHz, while the resonating frequency of TE_{01} mode is observed at 10 GHz (figure 3.6, 3.7). The stable operation of the amplifier is obtained by optimizing the total *Q*-factor of the dielectric-loaded cavity. The desired *Q*-factor of 252 is achieved by decreasing the electromagnetic energy inside the cavity with dielectric loading. Fourier transform of developed signal results the

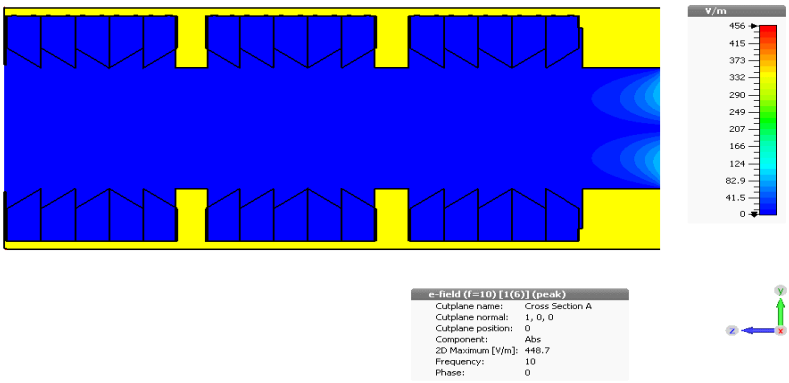

Figure 3.8 Electric field distribution in a drift tube

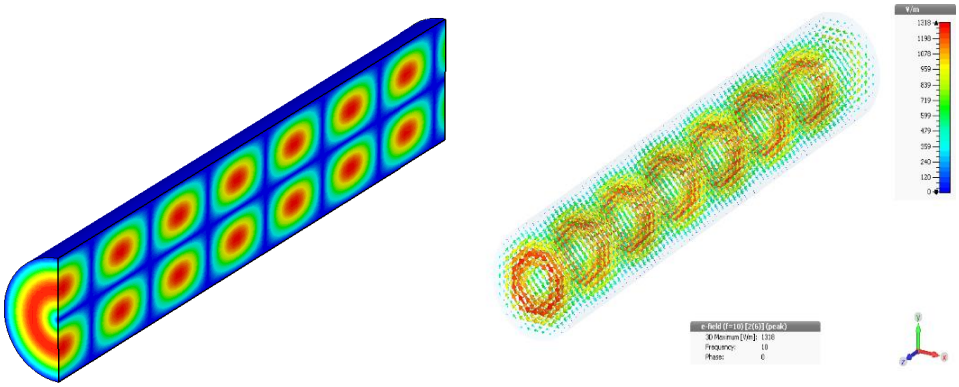

Figure 3.9 Field distribution in output waveguide section

resonant frequency of the cavity. Through the transient solver, the loss rate is calculated by measuring the S_{21}-parameter. Since, the drift tube is modelled to provide the isolation between cavity and waveguide, therefore, S_{21} -parameter of TE_{11} and TE_{21} are calculated as -61 dB and -53 dB, respectively. From the Figure 3.8, it can be seen that the electric field confinement is lowest in the drift tube region, which confirms the RF wave is well suppressed in the drift tube. Through the transient analysis of travelling wave section, its cut-off frequency is calculated for TE_{01} mode as 9.37 GHz. The electric field confinement confirms the propagation of TE_{01} mode in output travelling wave section (Figure 3.9).

3.3.3 PIC simulation

The 3D beam-wave interaction behaviour study of gyro-twystron has been made using the PIC solver of CST particle studio. Since the modelling of the cathode is possible with CST particle studio, therefore, modelling of the cathode is discussed in the present

section. Geometric parameters and beam parameters are fed through the predefined emission models to create the cathode. In tracking and PIC solver, a circular particle source with different emission models is chosen to create the cathode. A surface of PEC/non-PEC is picked to define the emitting face. Among the four-emission model, DC emission model is selected to define the kinetic parameters of the electron beam. The Energy, Lorenz factor, velocity and momentum are possible kinetic type, and the beam voltage is converted into any of the above-mentioned kinetic type to feed the kinetic value along with the total spread. The beam velocity pitch factor is converted to angle by taking the inverse of tangent and feed the DC emission model with the beam current. The value of outer and inner radii in circular particle source is equal to sum and difference of guiding centre radius and Larmor radius, respectively. PIC solver computes the particle dynamic in the presence of field as well as the calculated/updated field profile at small time interval using the leapfrog scheme. Time step in this self-consistent PIC simulation depends upon the size of the mesh step, which leads to a trade-off between simulation time and accuracy.

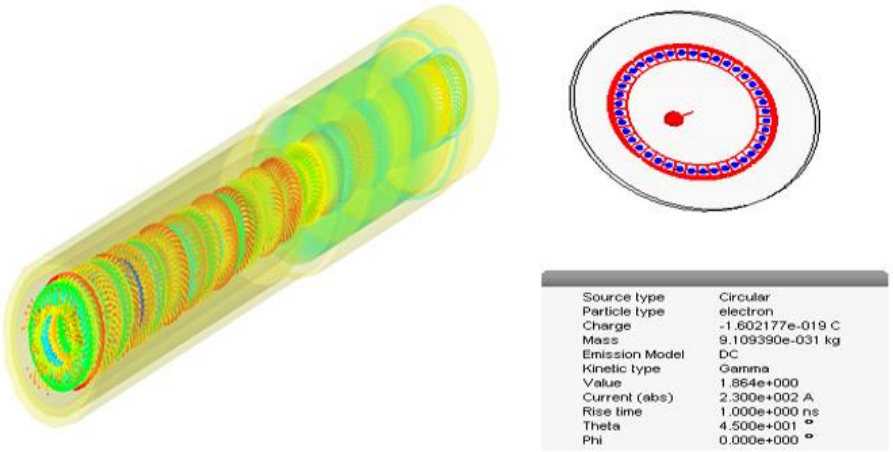

Figure 3.10 Particle perspective view of gyro-twystron with particle emitter model

The beam voltage of 440 kV is converted into velocity as a kinetic type, and unity pitch factor is converted into angle 45^0 using the inverse tangent of the pitch factor. The beam

parameters are borrowed from an experimental gyro-twystron[62], the electron beam having a beam voltage of 440 kV and beam current of 200-245 A, which is produced by magnetron injection gun. The value of outer and inner radii in circular particle source are 8 mm and 4 mm, respectively. With these parameters, the gyrating electron beam is reached at the input cavity and interacts with the applied RF input signal. The energy of electron particles is modulated by a signal in the input cavity, and with the inertia, electrons are getting ballistically bunched into field-free drift tube. These pre-bunched electron beam excites the RF wave in the output waveguide section nearly at cyclotron frequency. To amplify the RF power, the nonlinear interaction takes place in the output waveguide section. The energy of electrons at different position of the interaction structure is represented by energy colour ramp as shown in Figure 3.10, along with the beam parameters in the DC emission model. Based on the phase of transverse electric field and particle position, electrons are gaining and losing their energy, which leads to gain and lose their relativistic mass, respectively. Cyclotron frequency of heavier particle

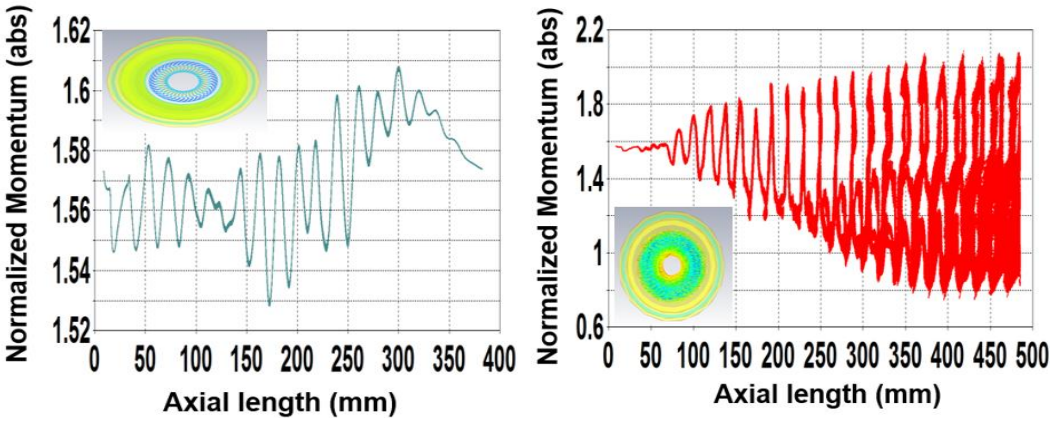

(a) (b)

Figure 3.11 Normalized momentum of particles Vs Axial length of gyro-twystron

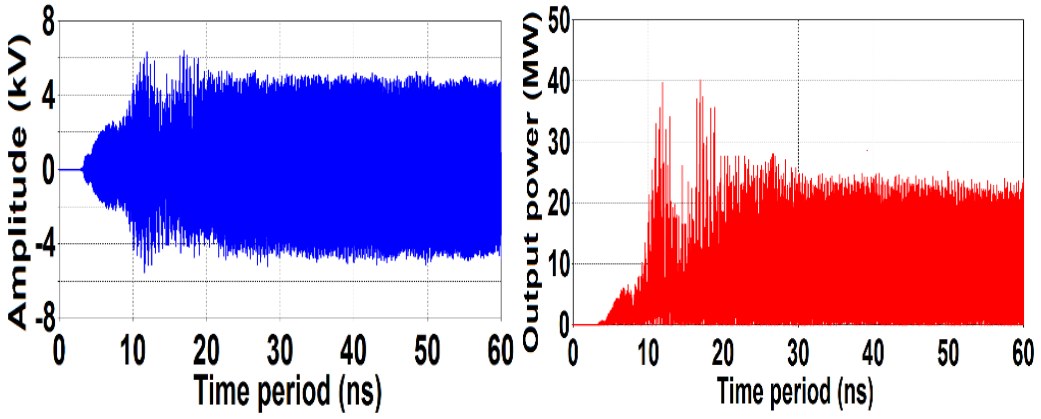

(a) (b)

Figure 3.12 (a) Temporal output signal response (b) the temporal output power growth TE_{01} mode

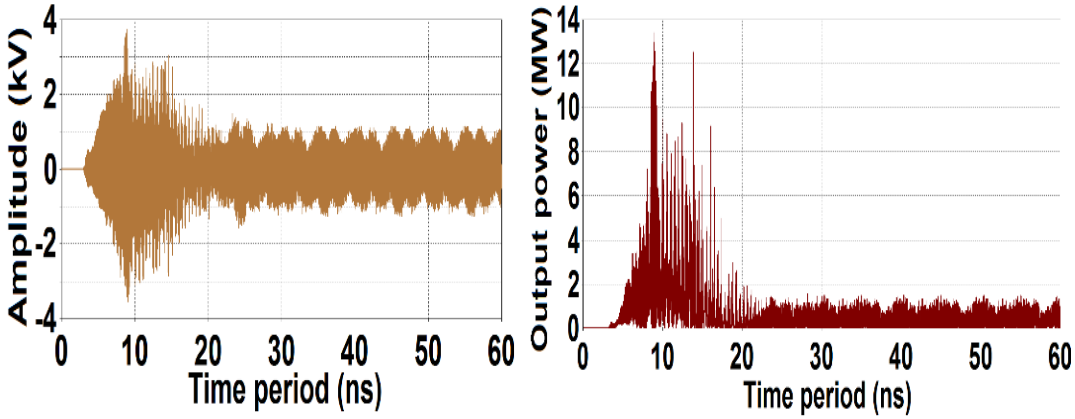

(a) (b)

Figure 3.13 (a) The temporal output signal response (b) the temporal output power growth TE_{02} mode

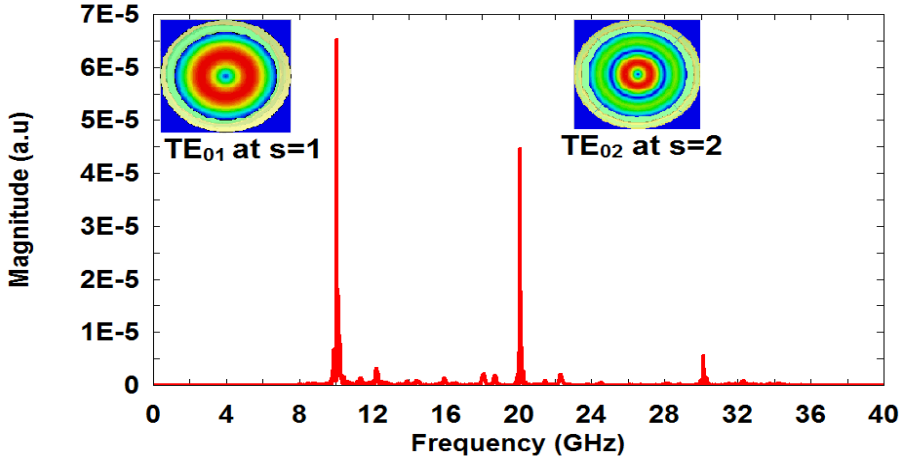

Figure 3.14 The frequency response of developed RF output power

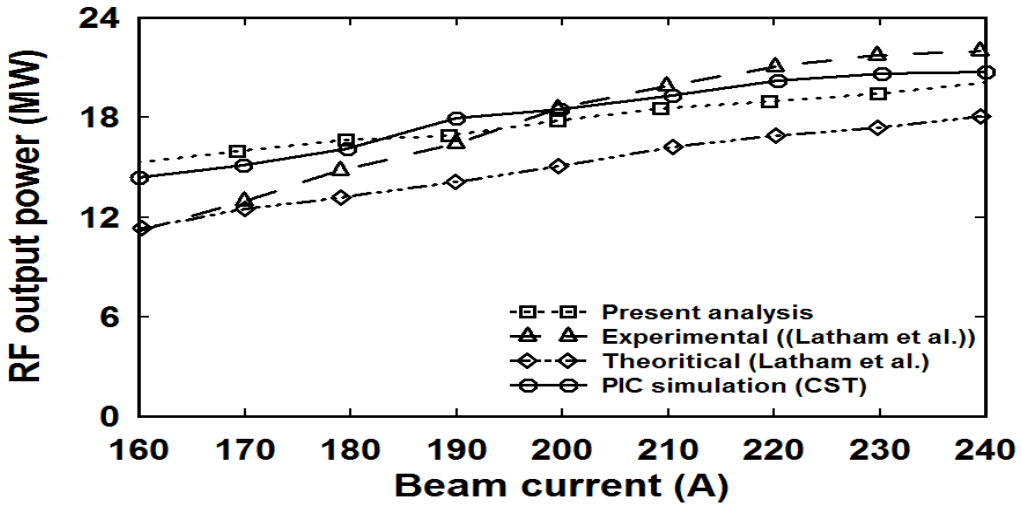

Figure 3.15 RF power variation over the beam current

is reduced, and the lighter particle is increased that leads to the phase bunching. The operating frequency is adjusted more than the cyclotron frequency for transferring the energy of particles to RF wave.

3.3.4 Result and discussion

Initially, the energy contained by all electrons remained the same around 440keV. The axial and orbital movement of particles have been observed at 2 ns (before bunching) and 60 ns (after bunching) of simulation time. Figure 3.11(a) shows the normalized axial momentum of particles at 2 ns along the axial direction of the RF circuit. The inner figure shows the corresponding transverse momentum of electrons. Similarly, Figure 3.11(b) shows the momentum at the end of the simulation. Initially, all particles travelled with a high angular velocity under the influence of a strong magnetic field with a normalized momentum of 1.57. The bunching occurs due to the variation of the Larmor radius of beamlets and the cyclotron frequency. This slows down the electron's velocity; hence, the angular momentum is reduced. The electrons tend to gyrate axially possess the kinetic energy in its transverse motion. This energy is converted into RF power. When a gyrating beam interacts with a fast EM wave in the presence of a strong magnetic field, it leads to an extraction of the transverse kinetic energy of electrons. According to Bremsstrahlung

radiation, the extraction of energy from the electron beam is possible only when the frequency of the RF signal is greater than the cyclotron resonance frequency of the beam. At the cyclotron resonance condition, the number of electrons gaining the energy is equal to the number of electrons losing the energy. Therefore, the net transfer of energy to the RF wave is almost zero. Figure 3.12(a) shows the peak value of the developed field amplitude of ~4.5kV at the output port in the desired TE_{01} mode. The direct square of this amplitude gives a saturated RF power of ~ 20MW, as shown in Figure 3.12(b). This is obtained through the post-processing feature of "CST particle studio" [96]. Similarly, the field amplitude and the corresponding power TE_{02}^{2} are shown in figure. 3.13(a) and 3.13(b), respectively. This shares more than 1 MW power and disturbs the stability to some extent. Other competing modes, including TE_{11} and TE_{21} are suppressed by taking the advantage of gradually tapered waveguide section used in the present simulation. However, the simulation predicts that this tapered waveguide is not capable of suppressing the TE_{02}^{2} .

Figure 3.14 shows the spectrum of the signal developed in TE_{01} mode (at s=1) with an operational frequency of 10 GHz at the output port. In addition, there is a signal associated with the second harmonic TE_{02} mode, which is closely competing with the operating mode. Figure 3.15 is the direct comparison of the present studies with the earlier experimental results [62]. However, the passing agreement between the present analytical and 3D PIC results due to the following reasons: 1) the peak power and the efficiency were limited by the parasites, and the degree of suppression of these modes is studied through the nonlinear, self-consistent, multimode code supports harmonics. To simplify the analysis, the following assumptions were made, including the absence of space charges, no drift in guiding centre radius, magnetic field and in-wall radius. Besides, at unity pitch

factor and currently higher than 200 A, the RF output power in the operating mode dominates over the parasites that lead to a significant error. 2) Beam loading in the PIC Simulation (hot simulation): it is a physical process in which the energetic gyrating electron beam and the RF electric field are interacting; conversely, the nonlinear 1-D results have been obtained by mere numerical calculations that do not have any loading. However, there is no big metric difference in the RF output power. The present 3D PIC simulation predicted ~20 MW of RF power in TE_{01} mode against analytical prediction of ~19.6 MW. These results are found to be in close agreement with the experimentally reported ~21 MW at the University of Maryland, the USA by Latham *et al* [62].

3.4 Conclusion

The beam-wave interaction behaviour of a gyro-twystron has been studied using a commercially available 3D PIC code CST particle studio. The simulation predicted a peak RF power of ~20 MW in the desired TE_{01} mode for the relativistic beam having 7 % velocity spread with a saturated gain of ~ 24 dB. The electronic efficiency was obtained as ~ 20 %, which is marginally less due to the self-start oscillation of TE_{02}^{2} in the output waveguide section. The 3-D beam wave interaction study along with the nonlinear transient behaviour of gyro-twystron has been benchmarked with an experimented device by Latham et al. at the University of Maryland as follows: (a) Latham et al. (experiment) Vs present nonlinear results agreed by 6 %. (b) Latham et al. (experiment) Vs 3D PIC results agreed by 5 %. In the present chapter, TE_{02}^{2} is identified is most troublesome mode, and the design calculation for suppressing TE_{02}^{2} mode will be an extension of the present work, which will be discussed in the next chapter.